Preparation and characterization of poly(vinylidene fluoride): A high dielectric performance nano-composite for electrical storage

CrossMark

S. Abdalla [a,*,1], A. Obaid [b,1], F.M. Al-Marzouki [a,1]

[a] Department of Physics, Faculty of Science, King Abdulaziz University Jeddah, P.O. Box 80203, Jeddah 21589, Saudi Arabia
[b] Department of physical chemistry, Faculty of Science, King Abdulaziz University Jeddah, P.O. Box 80203, Jeddah 21589, Saudi Arabia

ABSTRACT

We have prepared films of polymer nano-composite (PNC) of poly[vinylidene-fluoride] (PVDF) and bismuth vanadate ($BiVO_4$) nanoparticles. The α and γ electro-active phases were detected, and the addition of $BiVO_4$ drastically increases the formation of the α-phase. Addition of $BiVO_4$ produces up to 98% of electro-active phases. Robust electrostatic interactions arise between charges at the $BiVO_4$-surfaces, and differences in electron affinity between CH2 and CF2 groups created dielectric dipoles. The addition of $BiVO_4$ has not only enhanced the formation of the electrically active phases but also makes each dipole in the phase has its specific characteristics for example its own relaxation time. The AC-electrical permittivity showed that the dielectric constant of 10%wt- $BiVO_4$ nanoparticles in PVDF has a value 44 ε_0, which is four times more than the dielectric constant of the as-prepared PVDF films. These data show the importance of these polymers as easy, flexible, and durable energy storage materials.
© 2016 SA. Published by Elsevier B.V. This is an open access article under the CC BY-NC-ND license (http://creativecommons.org/licenses/by-nc-nd/4.0/).

Introduction

Lovinger [1] pioneered new polymer composites that are still attracting the interest of several researchers [2]. Kruusamäe et al. [3] have shown that electro-active polymers, in particular, have smart behaviors and different important applications: energy collection, biomaterials, sensors, actuators, etc. One of their interesting medical applications is their use as "artificial muscle" that behaves similar to real muscle. The material dilates when exposed to an external electric field, but shrinks when the electric field is removed. Thus, the electrical energy creates a mechanical force—this makes it a bio-transducer.

Poly-(vinylidene fluoride) (PVDF) has an excellent combination of different properties in addition to its semi-crystalline nature. While producing more progress in the energy-harvesting area, electro-active polymers are promising materials for effective energy harvesting. The development of several scientific studies can produce high and efficient investments in renewable energy domains and in the ascendant polymeric energy harvesters' technologies.

This material is an important technology with a promising future in actuator and electric energy generation. In addition, some

electro-active polymers have net piezo-, pyro- or ferro-electric properties such as the polyamide bio plastic Nylon-11 with superior thermal resistance [4]. Numerous electro-active polymers have shown different superior properties including poly(lactic acid) [5], poly-(lactic-co-glycolic) acid [6]. Concurrently, PVDF and its copolymers have excellent electro-active characteristics that vary depending on the internal structure. For example, by optimizing the geometry of PVDF chains and using quantum modeling calculations, Kepler [7] has demonstrated that different mean polarizabilities could be obtained depending on the vibrational-spectra that result from the interactions of the vibrational motions of the polymer chain. The mean value of the electrical dipole moment due to the monomer of the PVDF unit varies also from one electro-active phase to another: For both polymorphs the dipole moment per monomer unit converges to a nearly constant (5×10^{-3}°C.m for alpha-PVDF and 8×10^{-3}°C.m for beta-PVDF). Moreover, the magnitudes of the calculated dipole moment per monomer unit for a chain with 20 monomer units (5.2×10^{-3}°C.m for alpha-PVDF and 8.3×10^{-3} °C.m for beta-PVDF) are different from the value calculated from C–F and C–H bonds (7.0×10^{-3} °C.m).[7]. Adhikary et al. [8] have reported that the dipole moment arises essentially due to the high difference between the electronegativity of the fluorine atoms and other atoms such as carbon and hydrogen [8]. In these electro-active polymers, each chain has a dipole moment that is vertical to the chain itself. Due to different phases of PVDF, the beta phase has the highest dipole

---

moment per unit cell (8×10^{-3} °C.m [9]). The alpha and epsilon phases have no electrical activity because the packing of their dipole moment is anti parallel within the unit cell [10].

On the contrary, Rajesh et al. [11] have shown that the two active beta and gamma phases have a very high electro activity that makes them promising materials. These phases have serious applications in biomedicine [11], chemical warfare protection [12], batteries [13], sensors [14], actuators [15], magneto-electricity [16], filters [17], etc. Moreover, the gamma phase can store electric energy because of its strong dipole moments [18].

In addition, PVDF-nano-composites have received much recent attention due to their thermal, optical, electrical, dielectric, mechanical properties versus other smart materials, electro-active polymers are relatively cheaper, pliable, and easier to prepare. Thus, due to the importance of electro-activity, numerous techniques have been developed to obtain these phases, and different scenarios have progressed to get new electro-active polymers. Huge interest has been given to reveal the dielectric properties of PVDF polymers in order to potentiate implementations in energy storage applications [19–22]. However, the dielectric losses are highly reduced due to the presence of some "conducting-fillers" that decrease the electrical breakdown. So, several authors have used nano-ceramics as substitution filler material as they produce low dielectric losses due to their poor conducting properties [23]. These nano-ceramics ameliorate the electrical energy density of the composite and its hardness.

$BiVO_4$ has been chosen for two reasons: 1-Due to its narrow band gap (~2.3 eV – 43% of the solar spectrum), $BiVO_4$ has shown promised properties to be an excellent photo catalyst element which can be used for degradation of organics with promising applications notably in preserving the environment (obtaining clean water for example). 2-We were interested to examine the possibility whether addition of $BiVO_4$ to nano-composite polymer films of PVDF would change the dielectric properties of these films. In fact, we found that $BiVO_4$ improves the dielectric activity of the γ-phase in PVDF. This is due to the electrostatic interactions among the $–CH2–/–CF2–$ dipoles of PVDF and the delocalized π-electrons. Also, this is due to the remaining oxygen functionalities of Fe-doped RGO via ion–dipole and/or hydrogen bonding interactions [24].

As a future work and in order to get some natural, new and efficient polymers, we think to link flavonoid tannins to PVDF (long carbohydrate chains) [24–27]. This would open the doors to some sorts of new natural-smart materials that have the ability to store high energy density.

In the present study, we selected bismuth vanadate nanoparticles ($BiVO_4$-NPs) to be our filler material when preparation of PVDF nano-composite. $BiVO_4$-NPs stimulate the induction of electro-active phases (beta and gamma) in PVDF. Moreover, the dielectric properties of pure PVDF films have drastically improved upon addition of $BiVO_4$-NPs as filler. For example, the dielectric constant of pure PVDF is about 9 ε_0 at room temperature and 1 kHz; it increases markedly up to 44 ε_0 under the same conditions. This indicates that films of PVDF nano-composites are appropriate for energy storage across a vast range of frequency. For example, we have attained high values of energy density storage in PVDF nano-composites including 10.9 J cm^{-3} and losses of 4.9 J/cm^{-3}.

Experimental section

We used the following chemicals:

(1) Bi_2O_3 – Bismuth oxide with purity more than 99.9% – Finar Reagent
(2) V_2O_3 – Vanadium penta oxide with purity more than 99.9% – Loba Chemi
(3) PVDF – Beijing Star get New Materials Limited
(4) N,N-dimethylformamide – Beijing Star get New Materials Limited

Bismuth oxide Bi_2VO_3 was prepared as a nano powder starting with a mixture of solid materials and a suitable bowl grinding procedure as described previously [28]. It was then blended and milled with V_2O_5 in a one-to-one molar ratio followed by heating at 800 °C to get $BiVO_4$ powder. At ambient temperature, eight hours of mechanical milling with a Fritsch-Premium Line Pulveristte ball miller was needed to prepare nanoparticles of $BiVO_4$. To get the PVDF nano-composite films, we used a solvent solution containing $BiVO_4$ nanoparticles. The ratio between this and PVDF was 0.05, 0.1, 0.15 and 0.5. Before molding, we carefully kept the solution for ~30 min in an ultrasonic bath at 250 W to ensure homogeneous mixtures. The PVDF nano-composite was then prepared by propagating the solution on a suitable glass substrate followed by vacuum drying at 130 °C for six hours. The films were gently exfoliated from their substrates at the following ratios between $BiVO_4$:

(1) PVDF0 are films with no $BiVO_4$
(2) PNC4 are films with 5% $BiVO_4$
(3) PNC8 are films with 10% $BiVO_4$
(4) PNC16 are films with 15% $BiVO_4$
(5) PNC33 are films with 50% $BiVO_4$

Results and discussion

Characterization

Characterization experiments used 1-CuK-alpha X-ray diffraction radiation at 1.5406 Å run at 40 kV and 40 mA. This described the structure and the crystalline phases of the films. Fig. 1a shows the internal structure of the samples. The monochromatic Al K-alpha and a hemispherical photoelectron spectrometer analyzer SPECS Has 3500–1486.6 eV was also used. The diffraction pattern reveals the presence of several peaks corresponding to a single phase of monoclinic $BiVO_4$ because the XRD peaks nicely match JCPDS card number 75–2480. The Debye–Scherrer relation can estimate the nano-particle dimensions of $BiVO_4$ [29]: $L = \frac{0.9\lambda}{\Gamma_{FWHM} \cos\theta}$ is the width at 50% maximum of the different maxima. Our estimates lead to an average dimension of 8 nm when considering the three densest maxima. In addition, to identify the presence of crystalline phases in our materials, we used the X-ray diffraction data in Fig. 1b. This figure illustrates the diffraction patterns by X-ray of as prepared nano PVDF that will be denoted as PDV0 and films of polymer nano-composite with different concentrations of nanoparticles of $BiVO_4$ (within the PVDF-matrix) denoted as (PNC). The spectra of $BiVO_4$ nanoparticles are well manifested at two strong peaks at 18.6° and 28.8° that are shown in Fig. 1b.

The relative intensity of these two strong peaks in Fig. 1b and a are larger than that in Fig. 2a, which indicates that the polymer nano-composite films have more interactions between nanoparticles with PVDF molecules than those of PVDF0. Here, the PNC in the superficies of the nanoparticles are changed to better localizations. Moreover, the alpha crystalline phase in the PVDF nanoparticles is well manifested by the peaks at 17.6° for (100), 18.2° for (202), 19.8° for (110), and 26.2° for (021). Our data agree with published data [30].

Fig. 1b peaks show complete disappearance of the alpha peaks, but some new peaks are also created indicating the formation of both beta and gamma phases. In particular, the peak manifested at 18.2° completely superimposes the second strong diffraction peak of nanoparticles of $BiVO_4$. This is illustrated in the inset of
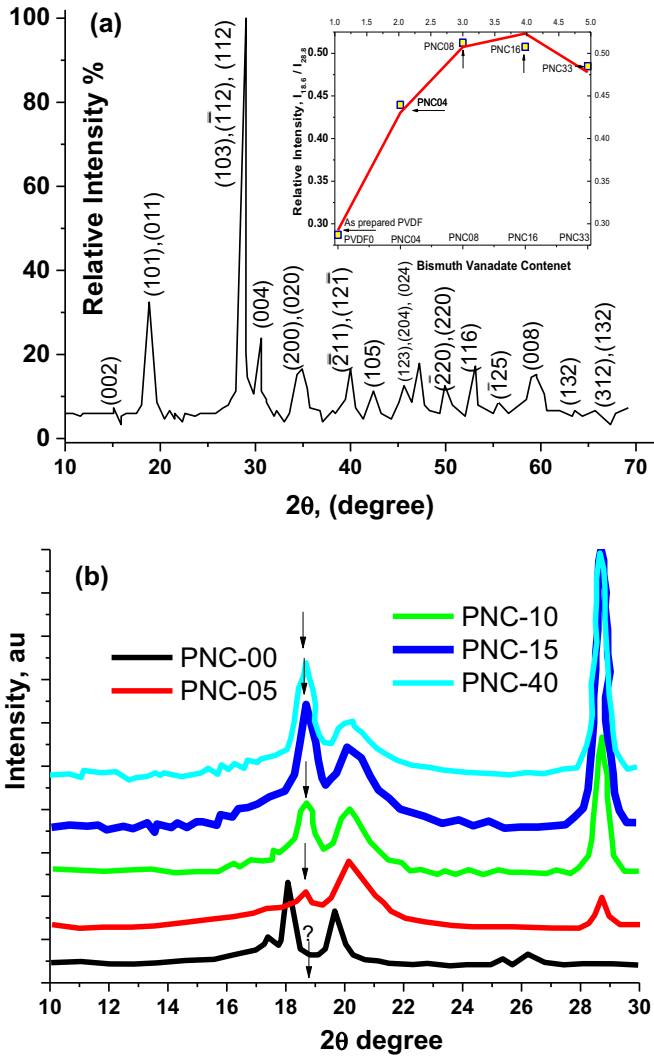
Fig. 1. (a) Diffraction-X-ray characteristics of as-prepared nano-particles of bismuth vanadate (BiVO₄). (b) Diffraction-X-ray characteristics of as-prepared PVDF (PVDF0) in addition to its films containing different contents of BiVO₄ (PNC). The characteristic-diffraction curve of bismuth vanadate is marked with arrow where it disappeared in PVDF-0.

Fig. 1b. This inset shows the normalized diffraction-X-ray characteristics of as-prepared PVDF (PVDF0) in addition to its films containing different contents of bismuth vanadate nanoparticles (PNC) with respect to the strongest peak at $2\theta = 18.6°$ and $28.8°$. Here, the ratio $R = I_{18.6}/I_{28.8}$ indicates the presence of the gamma phase. This will be further confirmed by Fourier transform inferred spectroscopy (FT-IR) data.

Fourier transforms inferred spectroscopy

Fig. 2a shows that PVDF0 has no non-electro-active alpha crystalline phase because of the strong absorption peaks at 976 cm⁻¹, 796 cm⁻¹, and 736 cm⁻¹. Here, the peak at 736 cm⁻¹ is the reference for identification of the alpha phase. One can notice the presence of two strong peaks at 1276 cm⁻¹ and 1232 cm⁻¹. This synchronizes with the beta and gamma phases, respectively. Seyhan et al. [31] have shown that the 840 cm⁻¹ peak has a dual feature in both beta and gamma phases. This was seen in our study. However, the alpha phase vanishes in the polymer nano-composite films and demonstrates how the presence of BiVO₄ is important in the crystalline phase transformation in PVDF films. That is, the FTIR
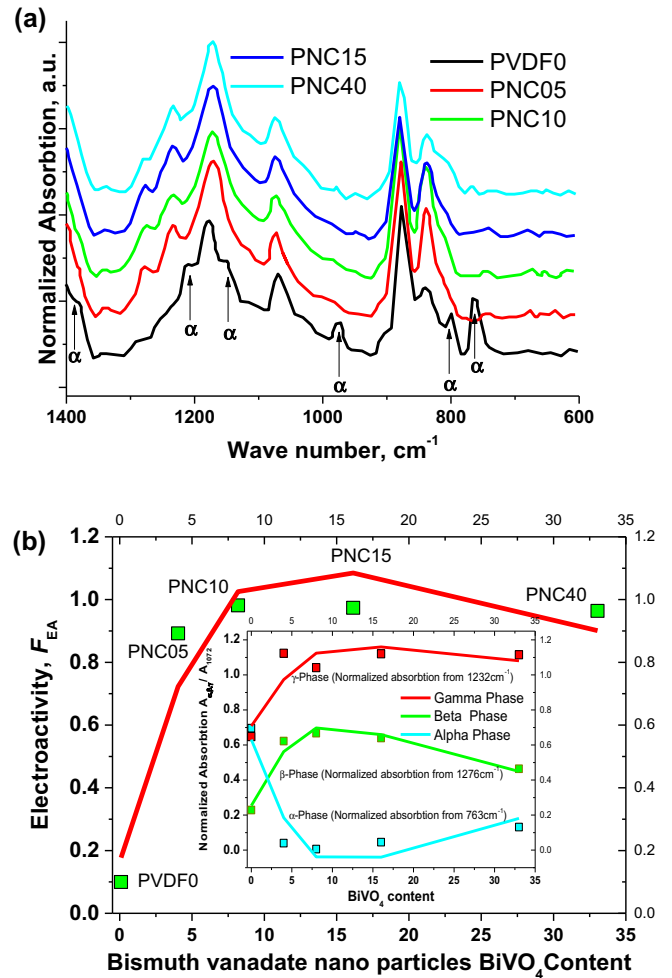

Fig. 2. (a) FT-IR spectroscopy of as prepared PVDF (PvDF0) and its films with different contents of bismuth vanadate nanoparticles. The alpha phase is marked by arrows. (b): Electro activity of different phases estimated from relation (1) as a function of different contents by wt% of BiVO₄ nanoparticles through PVDF matrix.

study shows the importance of the filler substance and that BiVO₄ nanoparticles ameliorate the electro-active properties of PVDF. Following Goncalves et al. [32] we have calculated the eventual content of the electro-active phase F_{EA} as follows:

$$F_{EA} = \frac{A_{EA}}{\left(\frac{k_{840}}{k_{736}}\right)A_{NEA} + A_{EA}} \tag{1}$$

where A_{EA} and A_{NEA} are the absorption strengths at 839 cm⁻¹ and 736 cm⁻¹.

Fig. 2b illustrates the electro-activity of F_{EA} as estimated from Eq. (1) as a function of BiVO₄—10% of BiVO₄ can create up to 98% electro-active phase, which clarifies the important role of bismuth vanadate to create new electro-active phases. The inset in Fig. 2b shows the variation of different phases (alpha, beta and gamma) through the polymer nano-composite film. In the inset of Fig. 2b, the normalized absorption strengths are illustrated as a function of the BiVO₄ content. The peak intensity at 763 cm⁻¹ corresponds to the alpha phase, the peak intensity at 1276 cm⁻¹ corresponds to the beta phase, and the peak at 1232 cm⁻¹ corresponds to the gamma phase. The reference is taken at 1072 cm⁻¹ for all normalization processes. We have chosen the line at 1072 cm⁻¹ because it is directly matched to our film-condensation regardless of PVDF crystalline changes. Also, this inset shows that the behavior of both beta and gamma phases are different than the alpha one. The

gamma phase suffers a minimum while the others (β and γ) have a maximum near 5% content of bismuth vanadate.

Model and interpretation: Dipole formation at the interface between PVDF and BiVO₄ nano particles

We studied the FTIR spectra of polymer nano-composite films to investigate the formation of different phases in PNC films and the formation of electro-active phases. We used the asymmetric ν_{as}–CH_2– and symmetric ν_{as} –CH_2– vibrating-bands from $3100\ cm^{-1}$ to $2900\ cm^{-1}$.

Fig. 3a demonstrates the interfacial interaction of different –CH_2– dipoles with the BiVO₄ nanoparticles. The arrows in Fig. 3a show the shift of ν_{as}–CH_2– vibrating bands to weaker energies in the polymer nano-composite film relative to the PVDF00 films. This confirms that the interfacial interactions between the polymer nano-composite film and the PVDF are very strong. This behavior has been reported by other authors [33–35]. As the BiVO₄ nanoparticle concentration increases, the shift (shown by arrows in Fig. 3a) increases as well—up to 15%; it then decreases.

The damped harmonic motion of –CH_2– dipoles is the reason for these shifts as demonstrated by Butt et al. [36]. The different electric charges on the exterior face of nanoparticles of BiVO₄ and –CH_2– stimulates the creation of electrostatic fields and electrostatic interactions that increase with BiVO₄ concentration. These interactions strongly resist the oscillations of –CH_2–; here, we calculate the damping coefficient r_{dc} from the relation:

$$r_{dc} = 4\pi C \sqrt{(\bar{\nu}_{NPVDF})^2 - (\bar{\nu}_{PNC})^2}.$$

Fig. 3b illustrates the dependence of this effect on concentration of BiVO₄ nanoparticles; the highest damping coefficient appears at PNC10. This is due to the percolation of BiVO₄ nanoparticles through the PVDF matrix. The content of the electro-active phase F_{EA} illustrated in Fig. 3b is similar to the damping coefficient r_{dc} shown in Fig. 3b. This consolidates the correlation between the electro-activity creation via PVDF and the surface charges on the BiVO₄ nano-particle. This behavior is schematically illustrated in the inset of the Fig. 3b. However, there are some exceptions where some segments of the PVDF chain are attracted to the charges on BiVO₄ nanoparticles. Others will be repelled because of the high inhomogeneities of the charge density allocations on the superficial domains of BiVO₄ nanoparticles.

X-ray Photoelectron Spectroscopy Analysis

Similar to Maji et al. [34], we studied the C1S and F1S – XPS spectra in PVDF matrix; high resolution spectra were obtained from the PVDF00 and PNC10 films. Clear maxima at 286.5 and 291.0 eV are seen in Fig. 4a indicating the presence of CH_2 and CF_2, respectively. A reasonable linking of 688.1 eV is seen in F1S and is illustrated in Fig. 4b. There is a clear difference in intensity (Δh_{CF2}) between the PVDF00 film and the PNC10 film as shown in Fig. 4a. This is due to a small CF_2 line when CH_2 was normalized. Fig. 4b illustrates the integrated-area-ratio (*IAR*) of the CH_2 (A_{CH2}) and CF_2 (A_{CF2}) groups. This *IAR* is equal in PVDF-nanoparticles, but it has been reduced by 5.5% in PNC10. We attribute this reduction in IAR to the CF_2 species [37,38]. An additional proof of the presence of interfacial interactions between BiVO₄ nanoparticles and PVDF nanoparticles is the small reduction in the ratio $\Delta R = \Delta (A_{CH2}/A_{CF2})$ of C1S of the PNC10 film with respect to PVDF nanoparticles. The reduction magnitude is about 9%. Fig. 4b shows that the line broadening is asymmetrical and that modification of the summit surface $\Delta (A_{F1S})$ is about 5%. Thus, one can use XPS data to conclude that there is interfacial interaction in PNC films with different concentrations of BiVO₄ nanoparticles. The same concentrations of BiVO₄ nanoparticles in Fig. 5c
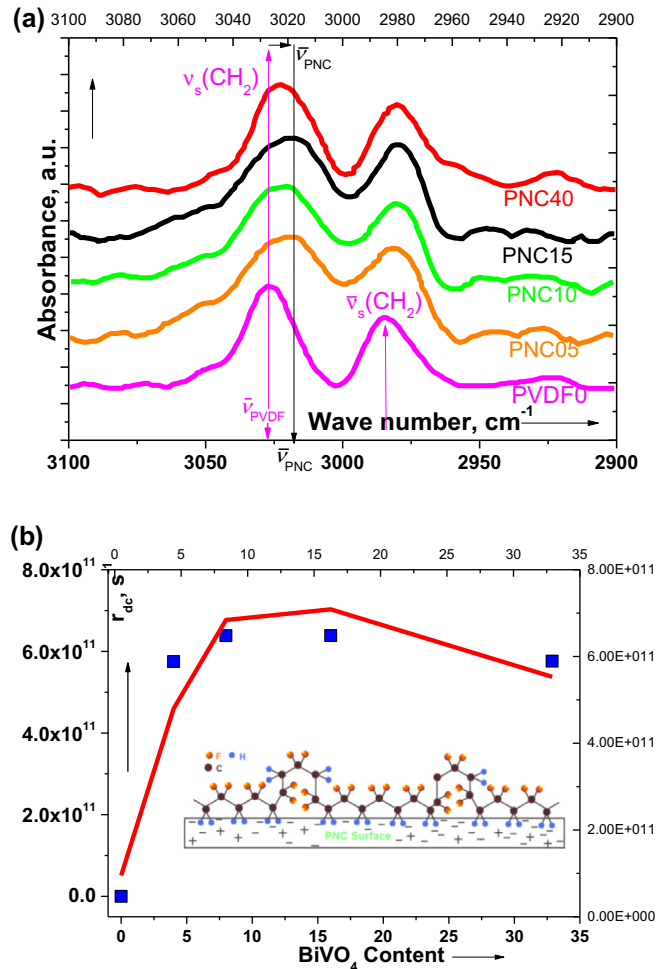

Fig. 3. (a) Fourier transformation (FTIR) results of as prepared PVDF and its corresponding BiVO₄ films from $3100\ cm^{-1}$ to $2900\ cm^{-1}$. (b) The damping parameter r_{dc} as a function of bismuth vanadate content in the PVDF matrix. The inset shows the formation of dipoles due to electrostatic interactions between the surface charge of nanoparticles and the surface of PVDF containing –CH2-CF2-dipoles.

show dependence of the electric losses ε'' as a function of frequency.

Dielectric behavior with addition of bismuth vanadate to PVDF

Fig. 5a shows the AC conductivity of polymer nano-composite films as a function of frequency f from $50\ Hz < f < 5 \times 10^6\ Hz$ for PVDF00, PNC05, PNC10, PNC10 PNC15, and PNC40. Fig. 5b illustrates the dielectric characteristics of polymer nano-composite films as a function of frequency for the same samples.

From the first sight, one can notice a gradual increase in the ac-electrical conductivity σ with frequency (Fig. 5a). The electrical conductivity varies with frequency according the power law $\sigma \alpha \omega^s$ [39] with a power factor s from $0 < s < 2$.

Fig. 5a shows that σ is divided into two main parts: In the first region, the dependence is in the form $\sigma \alpha \omega^{0.5}$ and in the second part; it increases as $\sigma \alpha \omega^{1.75}$ with a slight dependence on the concentration of BiVO₄ nanoparticles. The frequency at which these two regions meet is in the range $8 \times 10^3\ Hz < f < 1.5 \times 10^4\ Hz$ depending on BiVO₄ content. Fig. 5b shows the dielectric loss ε'' as a function of frequency in the same frequency range for different BiVO₄ content values. These curves show a common minimum in the frequency range $7.5 \times 10^3\ Hz < f < 2 \times 10^4\ Hz$ depending on the BiVO₄ content (Table 1).
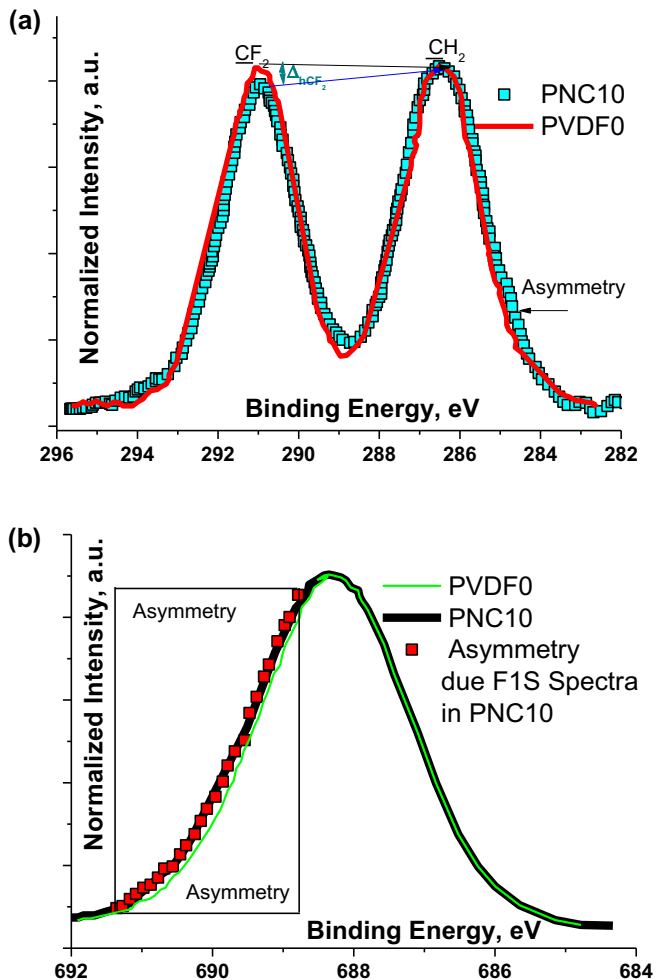
Fig. 4. (a) X-ray photoelectron spectroscopy spectra of as prepared PVDF and PVDF10 – polymer nano-composite film including high resolution C1 s spectra. The asymmetry due to F1s spectra in PNC10 film is indicated by an arrow. (b) XPS spectra of as prepared PVDF and PVDF10 – polymer nano-composite film including high resolution F1s spectra. The asymmetry due to F1s spectra in PNC10 film is indicated through the left rectangular area.

Table 1

reports the minimum values of dielectric losses and the corresponding critical frequencies f_c for different BiVO$_4$ content. The relaxation τ time is calculated after the relation: $\tau = 1/(2\pi f_c)$. Here, τ is the time necessary for charge to transfer from nanoparticles surfaces and the CH$_2$/CF$_2$ dipoles of PVDF.

BiVO$_4$ content	Minimum dielectric loss	Critical frequency f_c	Relaxation time, τ
0	0.00431974	7513.11	2.12×10^{-5}
5	0.00535075	16715.9	9.53×10^{-6}
10	0.00857109	20042	7.95×10^{-6}
15	0.00970104	10323	8.07×10^{-6}
40	0.00535075	16715.9	9.53×10^{-6}

In Fig. 5b, one can see that the dielectric constant for the composite PNC10 has the highest dielectric values and PVDF0 films are the lowest. This confirms that the addition of BiVO$_4$ increases the dielectric properties of PVDF. In general, the dielectric constant decreases with frequency for certain BiVO$_4$ contents, but here it varies with the BiVO$_4$ (Fig. 5c). The squares in this figure are the experimental values at certain frequency while the continuous line represents the calculated average value. The dielectric constant of the polymer composite films have a robust frequency dependence—they strongly decreases at low frequency range until

2 kHz and then suffer a soft decrease at higher frequencies. This is due to the electric polarization inside the matrix, which arises from the addition of BiVO$_4$ nanoparticles. The maximum dielectric constant is 58 ε_0 and 44 ε_0 at 50 Hz and 1 kHz, respectively, for PNC10. Here, ε_0 is the permittivity constant of the space.

The ε' of PNC05 is 4 times higher than that of PVDF0 films. This is in good agreement with the excellent electrical losses (Fig. 5c) that show promising materials for energy storage applications at different conditions. At low frequency, the strong dielectric values arise from direct polarization of the charge (Maxwell–Wagner polarization) via the interface between the PVDF matrix and the BiVO$_4$ nanoparticles (inset of Fig. 3b). In this figure, one can see that different traveler charges are created due to the polarization of the inorganic phase of the bismuth vanadate nanoparticles and the PVDF matrix. These charges arrange themselves in a minimum energy state as relaxed dipoles. The interfacial polarization arises at a low frequency because of the retardation of the relaxation motion of the created dipoles that increase the inertia of the dipoles. At higher frequencies, this is attributed to the formation of core–shell (surface functionalized nano-materials) through the PVDF matrix [40,41].

Sharma et al. [42] have shown that the addition of poly-methyl methacrylate (PMMA) to PVDF drastically affects the structural relaxations depending on the concentration of PMMA. A common minimum is observed in the dielectric curves of PVDF0 with PNC films at about 10 kHz. The dielectric losses of PVDF0 are nearly the same as those of PNC films. The different interactions inside the system PVDF matrix and BiVO$_4$ nanoparticles (inset of Fig. 3c) might create both interactions between nanoparticles and adjacent nanoparticles. They might also create different relationships between nanoparticles and polymers [43,44]. The crystalline size of the PVDF reduces when combined with BiVO$_4$ nanoparticles. The minimum dielectric loss in our study is found at 10% loading of BiVO$_4$ nanoparticles in the PVDF matrix. The minima frequencies ($f_{\min}$) at which the dielectric losses occur are a function of the BiVO$_4$ content. We calculated the relaxation time, τ of charges from the relation: $\tau = 1/(2\pi f_{\min})$.

Relaxation of dipoles due to addition of BiVO$_4$ to PVDF

The charge can be an electron the typical carrier, also, can be only a charge density ascribed to particular set of dipole under electric relaxation, but in movement also. In the first case, the long-range conductivity is operational, while in the second case, short-range conductivity is operational. Immediately above, there is a phrase from it is possible the follow interpretation: if electron can freely move by the materials, this material is not an ideal dielectric. This idea can be extended to materials that allow the electric dipole formation. Here, seems the proper moment to the parameter temperature exhibits all the power. A priori, the mobile charges are bonded to its proper defect or defect cluster that in a general way are thermal activated. This trend means that at each temperature a dielectric semiconductor or a dielectric with very slight semiconducting degree exhibits a value of real part of the complex dielectric permittivity and a value of imaginary part of dielectric permittivity. There is no universal role, instead there is a great number of variants, but as expected result when part real of dielectric permittivity increases, the correspondent imaginary part decreases and vice versa. Further picture can be reached with the material characterization as function of temperature. Here, it is important to have in mind that the concept of ideal dielectric was extended giving a new set of dielectric classification that was called dielectric-semiconductor (a dielectric with very slight degree of semiconducting properties). From this point, dielectric-semiconductors should be subdivided in two classes: The first class is represented by normal or conventional dielectric-semiconductors. Another class is of ferroelectric.

Ferroelectric is a particular dielectric that undergoes phase transition with changing of crystalline symmetry or space group or both, as a function of temperature. Thus, all ferroelectric is a dielectric-semiconductor normal but neither all dielectric-semiconductor normal is a ferroelectric. In addition, via over-simplification, the class called above of dielectric-semiconductor normal can be further mentioned in a simple way as dielectric. Then, all ferroelectrics are a dielectric but not all dielectrics are a ferroelectric. When both materials are characterized as a function of temperature, the major probability is that results are as follow: ferroelectric materials exhibit a complex behavior of parameter dielectric permittivity (real component of the complex number complex dielectric permittivity) being typical a maximum. Under temperature effects, dielectrics exhibit smooth curves sometimes with strong dispersion at low temperature (great values of dielectric permittivity). At a high temperature domain a strong dispersion of dipoles is detected. The overall behavior of dielectric permittivity parameter of dielectrics depends on the type and concentration of defects. By thermodynamic consideration, during measurements, defects are not being created, but can undergo ionization; electrons can be emitted or trapped. In this sense, as an example, in original state, oxygen vacancies should be in neutral state, as a function of temperature increasing, some ionization might take place providing further number of carriers. See, this meant that the electrical conductivity increases. See, the impedance is a complex function that can be transformed in electrical conductivity; in fact, the real part of electrical conductivity is a function of imaginary part of dielectric permittivity. In a polycrystalline materials are common both grain and grain-boundary phenomena. In a broad sense, being absent a universal role, the grain-boundary is a proper region to accumulate charge, also called space charge.

Applying these facts to our samples leads to the following: The fact that the concentration of BiVO$_4$-NPs filler is distributed at random all over the sample in the filler affects the resultant formation of electric dipoles and hence increases the net-polarization in the composites system. This leads to various relaxation times in whole PVDF-body. In another study, we have shown [45,46] that the random distribution of relaxation times is averaged to a most probable value with Gaussian distribution. The most probable value depends on several parameters such as morphology, temperature fine structure, etc. In the present samples, the "electric-inertia" of the formed dipoles in the PVDF-matrix results in a net extension of the polarization with respect to other dielectric process. This is translated by lowering of the dielectric constant, ε' in particular at high frequencies. On the contradiction, the strong lowering phenomenon of dielectric constant is not seen in neat-PVDF film. One can see that the composite with PNC10 has the most declared frequency dependence. In addition and more important, there are two net extra-humps that are clearly seen on Fig. 5b where we have pointed out by arrows. We have closely investigated the behavior of these humps as a function of different BiVO$_4$ concentrations and temperature. At three frequencies 100 Hz, 10 kHz and 1 MHz, Fig. 6 illustrates the variations of ε' as a function of different concentrations of bismuth vanadate within the PVDF matrix at 300 K. One can notice that the higher value of ε' is for the concentration PVDF-10. The experimental data of ε' at 10 kHz could be fitted to the empirical equation:

$$\varepsilon' = 2.778(C_{BiVO4}) - 0.6986(C_{BiVO4})^2 \qquad (3)$$

In Fig. 7a, we report the frequency dependence of the dielectric constant of PVDF-10 at 300 K for different concentrations of BiVO$_4$. The magnitude of the extra two humps varies gradually with the concentration of BiVO$_4$. One confirms the presence of maximum magnitude of ε' at PVDF10 and minimum at PVDF0 (neat sample). One notices that the two humps are quite weakened and even dis-
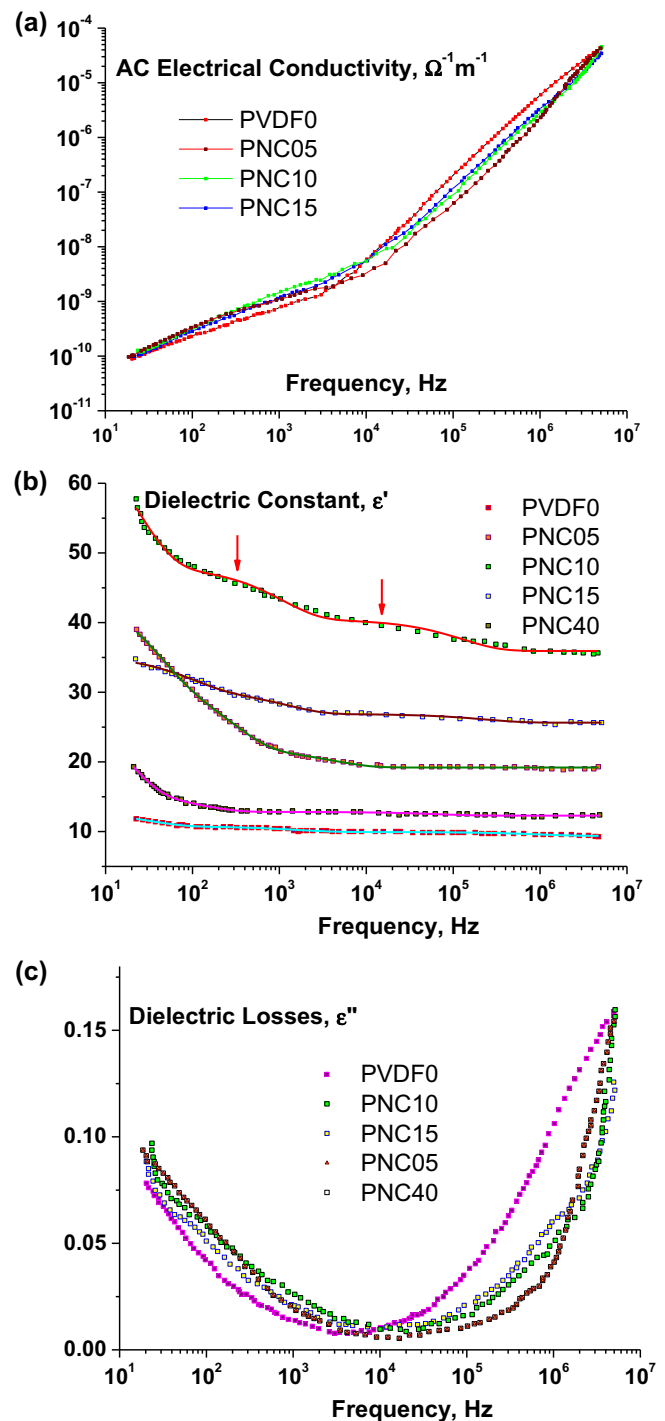

Fig. 5. (a) AC electrical conductivity as a function of frequency for different bismuth vanadate contents. (b) Dielectric constant as a function of frequency for different bismuth vanadate contents. (c) Dielectric losses as a function of frequency for different bismuth vanadate contents.

appeared at 400 K. This is attributed to the strong dispersion of relaxation times [45,46].

We were not sure whether these humps come from the experimental set up or from the samples themselves. Therefore, in order to be sure of our data, we measured ε' as a function of frequency and temperature and we present the experimental data in Figs. 8 and 9. The data in these figures give information about the relaxation of dipoles throughout the matrix.
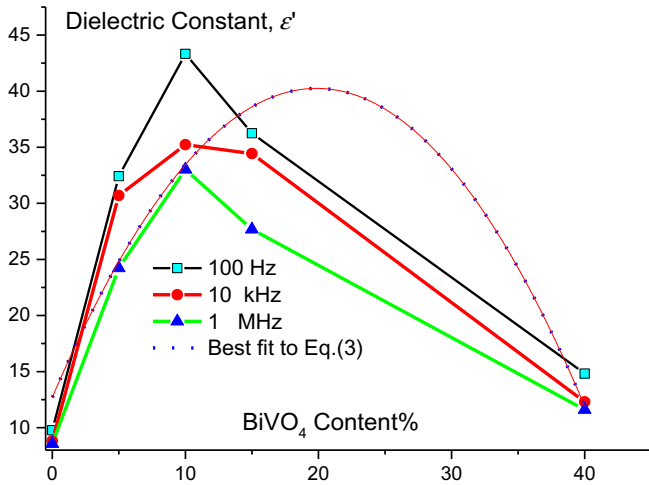
Fig. 6. Dielectric constant as a function of different contents of bismuth vanadate within the PVDF matrix at 300 K. The applied frequencies are 100 Hz, 10 kHz and 1 MHz. The dotted line represents the best fit of the curve – 10 kHz to Eq. (3): $\varepsilon' = 2.778(C_{BiVO4}) - 0.6986(C_{BiVO4})^2$ with CBiVO4 is the concentration of BiVO4 in the sample.

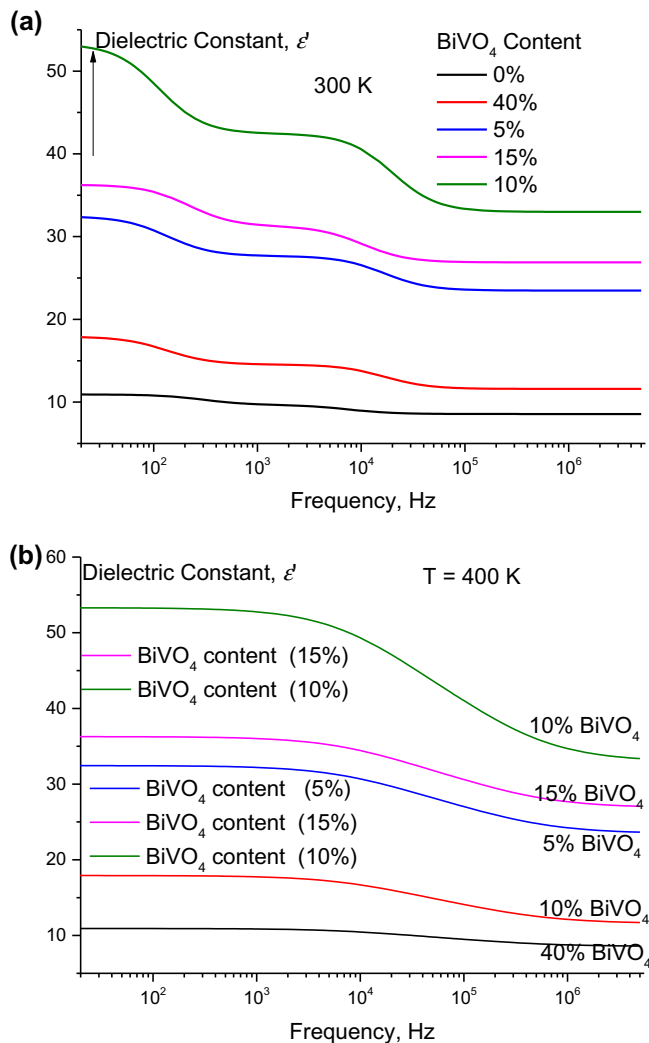**Fig. 7.** (a) At 300 K, dielectric constant, ε' as a function of the applied frequency for different concentrations of BiVO4. (b) At 400 K, dielectric constant, ε' as a function of the applied frequency for different concentrations of BiVO4.

As we see in Fig. 8, ε' moves gradually toward higher frequencies with temperature. In order to explain this behavior, we consider the following model:

(1) The presence of dipoles created due to the difference between electron affinities of fluoride and carbon atoms. [47,48]

(2) These dipoles relax obeying Debye mechanism [49] with relaxation time τ,

(3) After Debye model, the dielectric constant and electrical conductivity σ is given as:

(4)
$$\varepsilon' = \varepsilon_\infty + \frac{(\varepsilon_{dc} - \varepsilon_\infty)}{1 + \omega^2\tau^2} \text{ and } \sigma = \sigma_{dc} + \omega^2\tau\frac{(\varepsilon_{dc} - \varepsilon_\infty)}{1 + \omega^2\tau^2} \qquad (4)$$

where ω is the angular frequency $\omega = 2\pi f$, ε_{dc} is the dielectric constant at very low frequencies (dc-conditions), ε_∞ is the dielectric constant at very high frequencies. σ_{dc} is the electrical conductivity at very low frequencies (dc-conditions),

(5) These two equations fit well experimental data in Figs. 8 and 10 with the following fitting parameters:

(6) $\sigma_{dc} = \sigma_{dc0} \exp\frac{-(\Delta E)}{kT}$ and $\tau = \tau_0 \exp\frac{\Delta E}{kT}$ ΔE is a thermal activation energy; σ_{dc0} and τ_{dc0} are fitting parameters.

$$\varepsilon_{dc} = \tau_0\sigma_{dc0} \text{ and } \varepsilon_\infty = \tau_0\sigma_{dc0} \exp\frac{-(\Delta E)}{kT}$$

(7) The surface area between the polymer matrix and BiVO4 molecules is constant. Therefore, there are certain specific numbers of dipoles that can be attached by filling this area. However, adding more dipoles (by increasing the BiVO4 concentration) will create destructive electrical interference between the present dipoles and added ones. This leads to attenuation of dielectric polarization and consequently it leads to reduction of dielectric constant. This explains why the dielectric constant decreases with increasing BiVO4 concentration.

(8) After these analyses, the previously observed two humps are corresponding to two relaxation phenomena due to the presence of two different phases in our samples: alpha and beta. Ozkazanc et al. [50] reported the same behavior for BiVO4.

(9) Moreover, the previously observed two humps are corresponding to two relaxation phenomena due to the presence of two different phases in our samples: alpha and beta. Ozkazanc et al. [50] have reported that the curve describing the dielectric loss factor as a function of temperature, of α-phase PVDF, suffers a maximum at 285 K (at 5 kHz). While this maximum attains 390 K (at 5 kHz) for β-phase PVDF [50]. Therefore, we can attribute the relaxation phenomenon that we have observed with activation energy of 0.6 eV is due to relaxation of dipoles in α-phase while these with activation energy of 0.3 eV is due to relaxation of dipoles in β-phase.

(10) In Fig. 10, we report the relaxation time of α - and β-dipoles as a function of the BiVO4 concentration. The empirical equations that lead to the best fitting parameters to fit the relaxation times of both phases are as following:

$$\tau_\alpha = 4.74 - 0.408(C_{BiVO4}) + 8.488(C_{BiVO4})^2 \qquad (5)$$

$$\tau_\beta = 3.27 + 0.112(C_{BiVO4}) - 0.009(C_{BiVO4})^2 + 1.72(C_{BiVO4})^3 \qquad (6)$$

It is well seen that the frequency dependence of dielectric permittivity is highly manifested through the total frequency range in the PNC10 sample that may be attributed to the orientation of electrically active dipoles that reduces the specific volume in the amorphous phase. The formation of hollow
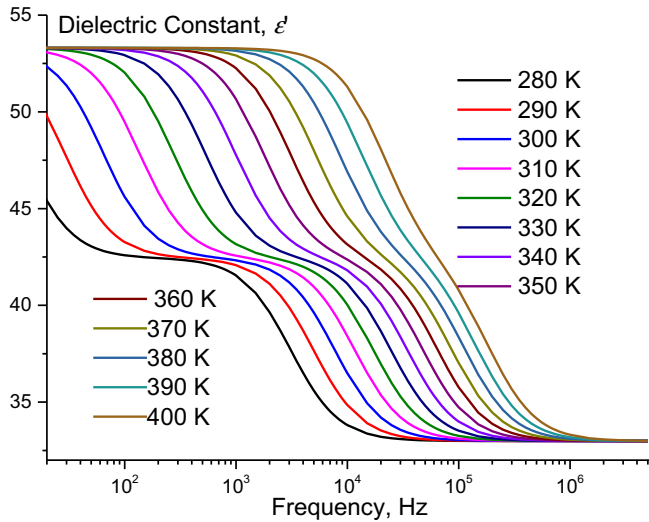
Fig. 8. Dielectric constant, ε' as a function of the applied frequency at different temperatures; for PVDF-10.
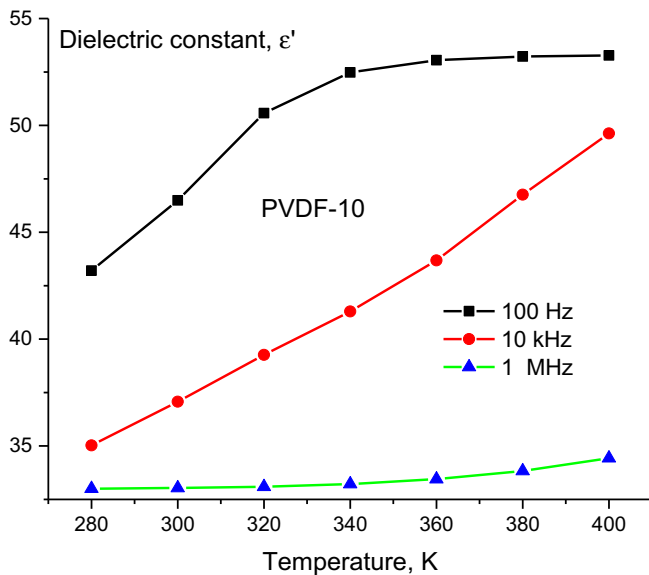

Fig. 9. Dielectric constant, ε' as a function of the temperature for frequencies at 100 kHz, 10 kHz and 1 MHz; for PVDF-10.

Fig. 10. Relaxation time of charge dipoles as a function of bismuth vanadate contents. Black squares represent the relaxations due to α-phase. Red line is the best fit of relaxation times to Eq. (5). Red circles represent the relaxations due to β-phase. Blue line is the best fit of relaxation times to Eq. (6). (For interpretation of the references to color in this figure legend, the reader is referred to the web version of this article.)

spherical structures stimulates creation more dipoles in the PNC10 film. This type of frequency dependency of the dielectric constant is similar to core–shell or surface functionalized nanoparticle added PVDF films. Sharma et al also observed this behavior [51]. More interestingly the dielectric loss in all the PNC films is lower than that of the neat-PVDF films in higher frequency region (>10 kHz). In addition, at 10 kHz, the dielectric loss is very close to that of the pure PVDF film and the loss is significantly lower with respect to its dielectric constant (Fig. 5c). In our case, we found that the minimum dielectric loss occurs at 10 wt% loading of BiVO$_4$-NPs into PVDF solution.

Surface polarization is a natural consequence for the presence of different relaxation times in PVDF matrix and inorganic phase of BiVO$_4$-NPs. This forms an important number of dipoles.

In addition, more dipoles will be added within the BiVO$_4$ nanoparticles because its dimension is about 7 nm. The dielectric-inertia of the created dipoles in the PNC samples gives a prolongation of t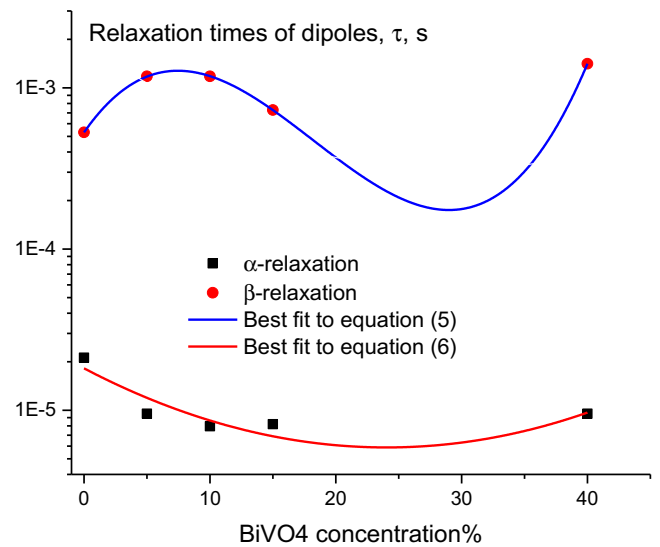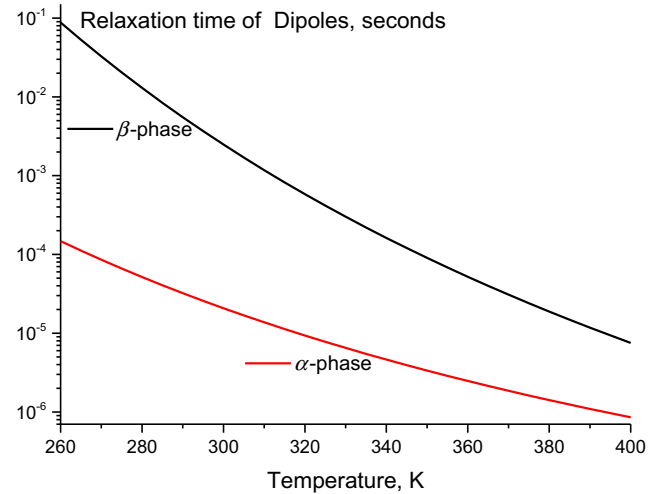he polarization in comparison to other dielectric process, which favors the interfacial polarization at low frequencies. Therefore, the dielectric constant decreases rapidly at higher frequencies. However, the decay of dielectric constant is absent in NPVDF film which reflects the minor number of dielectric dipoles. This makes the frequency dependence of dielectric permittivity not sufficiently manifested over the entire frequency domain in the neat PVDF samples.

(11) Fig. 11 shows the temperature dependence of the relaxation time for both alpha and beta-phases. The relaxation time obeys Eq. (6) with the parameters stated in Table 2.

(12) In fact, we need to carry out more fine experimental-data in order to find the exact concentration at which dipoles attain their maximum. This will be in a future study.

Energy storage efficiency with addition of bismuth vanadate to PVDF

Fig. 11a illustrates the electric displacement, D as a function of the applied electric field for different contents by weight of bismuth vanadate: 0%, 5%, 50%, 15% and 10% within PVDF matrix
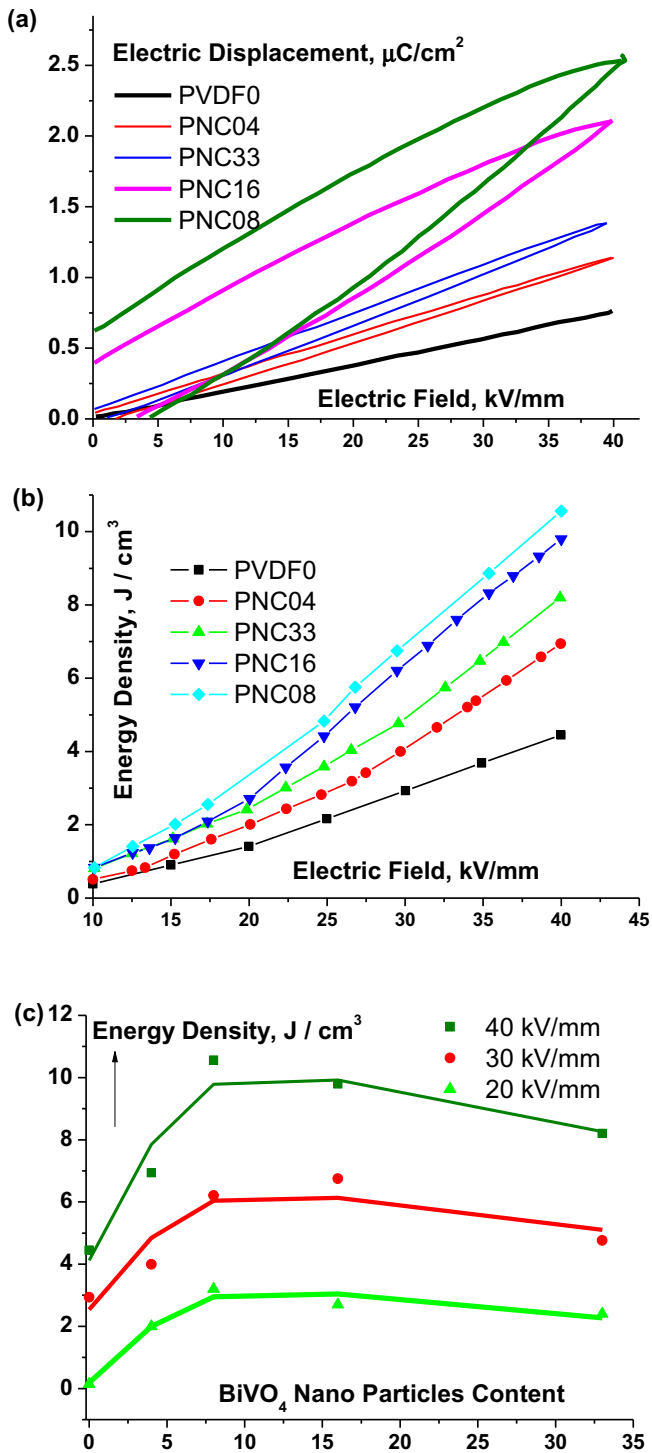
Fig. 11. (a) Electric displacement, D as a function of the applied electric field for different contents of bismuth vanadate within the PVDF matrix (D-E loops). (b) The energy density as a function of the applied electric field for different contents of bismuth vanadate within PVDF matrix (c). Energy density is illustrated as a function of the contents of bismuth vanadate within PVDF matrix for different applied electric field.

(D-E loops). The maximum lies at PNC10, which corresponds to a maximum polarization of 0.071 C/m² for PNC10. The electric displacement increases markedly with addition of BiVO$_4$ nanoparticles until 10% and it then decreases. Fig. 11b illustrates the energy density as a function of the applied electric field for different contents of bismuth vanadate within the PVDF matrix. This figure shows that the composition "PNC10" attains a value

Table 2
shows the most suitable fitting parameters that fit the experimental data to Eq. (4) at 300 K.

% BiVO$_4$	ΔE, eV (τ_0, seconds)		$\sigma_{dc0}\ \omega^{-1}\,m^{-1}$
	α-Phase	β-Phase	
0	–	–	0.000614
5	0.6 (6.4×10^{-11})	0.3 (2.1×10^{-13})	0.000805
10	0.6 (6.4×10^{-11})	0.3 (2.1×10^{-13})	0.000654
15	0.6 (6.4×10^{-11})	0.3 (2.1×10^{-13})	0.000694
40	0.6 (6.4×10^{-11})	0.3 (2.1×10^{-13})	0.000804

of 10.37 J/cm³ when the applied electric field is about 40 kV/mm and Fig. 11c shows the energy discharge density U_d as a function of the BiVO$_4$ nanoparticles for different values of the electric field; PNC10 shows maximum energy storage. The energy density $\mathcal{J}$ is given by definition as [52] $\mathcal{J} = \int_{D_r}^{D_{max}} EdD$ where D_r and D_{max} are the remnant and maximum electric displacement respectively. The addition of BiVO$_4$ has enhanced the formation of the electrically active β-phase in addition to the previously found phases. This makes energy storage efficiency cannot be give out. This can be estimated from the loops in Fig. 11a [53,54]. The energy density of PNC10 films is 10.37 J/cm⁻³ with an energy loss 4.9 J/cm⁻³. This is one of the best PVDF-polymers. This material could be used in rechargeable batteries.

Conclusions

Strong electro-active phases are formed when bismuth vanadate nanoparticles (BiVO$_4$) are added to poly[vinylidene-fluoride] (PVDF). The dielectric properties of PVDF increase with BiVO$_4$-nano-doping. Robust electrostatic fields arise in the polymer nano-composite (PNC) films due to strong interactions between charges on the BiVO$_4$ nanoparticles and induced dipoles on the PVDF matrix. Low dielectric losses with relatively high dielectric constant have been found when adding 10 wt% nanoparticles to PVDF across a wide range of frequencies (kHz to MHz). This polymer is a candidate material for future electronic devices—especially those needing storage in high energy flexible systems. The addition of BiVO$_4$ has not only enhanced the formation of the electrically active phases but also makes each dipole in the phase has its specific characteristics for example its own relaxation time. The remarkably low energy loss in the PNC films with high energy storage meets the demands of future applications in different domains including the following: high-energy, elastic film type capacitances; materials with high k-parameters for use in field-effect transistors; pulsed power-generators; and power conditioning.

Author contributions

F.A. conceived and designed the experiments; S.A. performed the experiments; S.A. and A.O. analyzed the data; F.A. contributed reagents/materials/analysis tools; A.O. and S.A. wrote the work.

Conflicts of interest

The authors declare no conflict of interest.

Acknowledgments

References

[1] Lovinger AJ. Ferroelectric polymers. Science 1983;220:1115–21.

[2] Yoseph Bar-Cohen, Electro-active polymer actuators and DEVICES (EAPAD) Proc. SPIE 9430, 2015, 943001; doi: http://dx.doi.org/10.1117/12.2184300.

[3] Kruusamäe K, Punning A, Aabloo A, Asaka K. Self-sensing ionic polymer actuators: a review. Actuators 2015;4:17–38. http://dx.doi.org/10.3390/act4010017.

[4] Jinhong Y, Huan X, Wu C, Jiang P. Permittivity, thermal conductivity and thermal stability of poly(vinylidene fluoride)/graphene nanocomposites. IEEE Trans. Dielectr. Electr. Insul. 2011;8(2):478–84.

[5] Jamshidian M, Tehrany EA, Imran M, Jacquot M, Desobry S. Poly-lactic acid: production. Applications, nanocomposites, and release studies. Comp. Rev. Food Sci. Food Saf. 2010;9:552–71.

[6] Kosinski AM, Brugnano JL, Seal BL, Knight FC, Panitch A. Synthesis and characterization of a poly (lactic-co-glycolic acid) core poly(N-isopropylacrylamide) shell nanoparticle system. Biomatter 2012;2(4):195–201. http://dx.doi.org/10.4161/biom.22494.

[7] Piezoelectricity Kepler RG. Pyroelectricity and ferroelectricity in organic materials. Ann. Rev. Phys. Chem. 1978;29:497–518.

[8] Adhikary P, Garain S, Mandal D. The co-operative performance of a hydrated salt assisted sponge like P (VDF-HFP) piezoelectric generator: an effective piezoelectric based energy harvester. Phys. Chem. Chem. Phys. 2015;17:7275.

[9] L. Yu, P. Cebe, Effect of nanoclay on relaxation of poly (vinylidene fluoride) nano composites, J. Polym. Sci, 2520–2532.

[10] S.M. Damaraju, Siliang Wu, M. Jaffe, T. Livingston, Arinzeh, Structural changes in PVDF fibers due to electrospinning and its effect on biological function, Biomed. Mater. 8 (2013) 045007 doi: http://dx.doi.org/10.1088/1748-6041/8/4/045007.

[11] Rajesh PSM, Bodkhe Sampada, Kamle Sudhir, Verma Vivek. Enhancing beta-phase in PVDF through physicochemical modification of cellulose. Electron. Mater. Lett. 2014;10(1):315–9.

[12] Thakur P, Kool Arpan, Bagchi Biswajoy, Das Sukhen, Nandy Papiya. Enhancement of β phase crystallization and dielectric behavior of kaolinite/halloysite modifid poly (vinylidene fluoride) thin films. Appl. Clay Sci. 2014;99:149–59.

[13] Hong Liang, Rodrigo Cooper, Jason Files, Phase transformation of poly (vinylidene difluoride) in energy harvesting, J. Mater. Res. 26(1) (Jan 14, 2011), 1–8.

[14] V. Patil, A. Jain, Design of stretching unit for continuous? Phase PVDF film and analysis of piezoelectric film sensor for transducer applications, Int. J. Eng. Res. Technol. 2(12), 2013, e-ISSN: 2278–0181.

[15] Yamakita M, Kamamichi N, Kaneda Y, Asaka K, Luo Z. Development of an artificial muscle linear actuator using ionic polymer–metal composites. Advanced Robotics, Springer 2004;18(4):383–99.

[16] Carvell Jeffrey, Cheng Ruihua, Yang Q. Induced magneto-electric coupling at ferroelectric/ferromagnetic interface. J. Appl. Phys. 2013;113:17C715. http://dx.doi.org/10.1063/1.4794873.

[17] Muhamad Nasir, Hidetoshi Matsumoto, Mie Minagawa, Akihiko Tanioka, Tetsuya Danno, Hideo Horibe, Formation of beta-phase crystalline structure of PVDF nano fiber by electrospray deposition: additive effect of ionic fluorinated surfactant, Polym. J. 39(7), (2007), 670–674.

[18] Vinogradov AM, Schmidt HV, Tuthill GF, Bohannan GW. Damping and electromechanical energy losses in the piezoelectric polymer PVDF. Mech. Matls. 2004;36:1007–16.

[19] Garain S, Sinha TK, Adhikary P, Henkel K, Sen S, Ram S, Sinh C, Schmeisser D, Mandal D, Appl ACS. Mater. Interf. 2015;7:1298–307.

[20] Sharma M, Madras G, Bose S. Unique nano-porous antibacterial membranes derived through crystallization induced phase separation in PVDF/PMMA blends. J. Mater. Chem. A 2015;3:5991–6003. http://dx.doi.org/10.1039/C5TA00237K.

[21] Sharma M, Sharma K, Bose S. Segmental relaxations and crystallization-induced phase separation in PVDF/PMMA blends in the presence of surface-functionalized multiwall carbon nanotubes. J. Phys. Chem. B 2013;117(28):8589–602. http://dx.doi.org/10.1021/jp4033723.

[22] Madras, Bose S, Sharma M. Contrasting effects of graphene oxide and poly (ethylenimine) on 2 the polymorphism in poly(vinylidenefluoride). Cryst. Growth Des. 2015. http://dx.doi.org/10.1021/acs.cgd.5b00445.

[23] Bedilu A. Allo, Daniel O. Costa Bioactive, S. Jeffrey Dixon, Kibret Mequanint, Amin S. Rizkalla, Biodegradable nanocomposites and hybrid biomaterials for bone regeneration, J. Funct. Biomater. 3 (2012), 432–463, doi: http://dx.doi.org/10.3390/jfb3020432.

[24] Karan SK, Mandal D, Khatua BB. Self-powered flexible Fe-doped RGO/PVDF nanocomposite: an excellent material for a piezoelectric energy harvester. Nanoscale 2015 Jun 28;7(24):10655–66. http://dx.doi.org/10.1039/c5nr02067k.

[25] Abdalla S, Pizzi A, Ayed N, Charrier F, Bahabry F, Ganash A. MALDI-TOF and 13C NMR analysis of Tunisian Zyzyphus jubjuba root bark tannins. Ind. Crops Prod. 2014;59:277–81.

[26] Maria Cecilia Basso, Antonio Pizzi, Clement Lacoste, Luc Delmotte, Fahad M. Al-Marzouki, Soliman Abdalla, Alain Celzard, MALDI-TOF and 13C NMR analysis of Tannin–Furanic–Polyurethane foams adapted for industrial continuous lines application, Polymers 6 (2014), 2985–3004. doi: 10.3390/polym6122985.

[27] Abdalla S, Pizzi A, Ayed N, Charrier F, Bahabri F, Ganash A. MALDI-TOF and 13C NMR analysis of Tunisian Zizyphus jujuba root bark tannins. Ind. Crops Prod. 2014;59:277–81.

[28] A.V. Egorysheva, V.D. Volodin, O.G. Ellert, N.N. Efimov, V.M. Skorikov, A.E. Baranchikov, V.M. Novotortsev, Mechanochemical activation of starting oxide mixtures for solid state synthesis of BiFeO₃, SSN 00201685, Inorg. Mater. 49(3), (2013)303–309. © Pleiades Publishing Ltd, 2013.

[29] Taylor A, Sinclair H. On the determination of lattice parameters by the debye-scherrer method. Proc. Phys. Soc. 1945;57:126. http://dx.doi.org/10.1088/0959-5309/57/2/306.

[30] Buckley J, Ceb P, Cherdack D, Crawford J, Seyhan Ince B, Jenkins Matthew, Pan Jenkins, Reveley Matthew, Washington Niesha, Wolchover Natalie. Nanocomposites of poly(vinylidene fluoride) with organically. Polymer 2006;47:2411–22.

[31] Seyhan B, Ince-Gunduza, Burkeb Kristina, Koplitzc Michelle, Meleskib Matthew, Meleskib Ari, Sagivd Ari, Cebea Peggy. Impact of nanosilicates on poly (vinylidene fluoride) crystal polymorphism: part 2. Melt-crystallization at low supercooling. J. Macromol. Sci. Part A 2010;47:12.

[32] Gonçalves R, Martins P, Moya X, Ghidini M, Sencadas V, Botelho G, Mathurd ND, Lanceros-Mendez S. Magneto-electric CoFe₂O₄/polyvinylidene fluoride electro-spun nano fibers. Nanoscale 2015;7:8058.

[33] Sharma T, Naik S, Langevine J, Gill B, Zhang JX. Aligned PVDF-TrFE nanofibers with high-density PVDF nanofibers and PVDF core–shell structures for endovascular pressure sensing. IEEE Trans. Biomed. Eng. 2015 Jan;62(1):188–95.

[34] Maji S, Sarkar PK, Mandal D, Sheet G, Aggarwal L, Ghosh SK, Achary S. Self-oriented b-crystalline phase in the polyvinylidene fluoride ferroelectric and piezo-sensitive ultrathin Langmuir-Schaefer film. Phys. Chem. Chem. Phys. 2015;17:8159–65.

[35] Tan KS, Gan WC, Velayutham TS, Abd Majid WH. Pyro-electricity enhancement of PVDF nano composite thin films doped with ZnO nanoparticles. Smart Mater. Struct. 2014;23:125006.

[36] Butt H-J, Cappella B, Kapp M. Force measurements with the atomic force microscope: Technique, interpretation and applications. Surf. Sci. Rep. 2005;59:1–152.

[37] Ying L, Wang P, Kang ET, Neoh KG. Synthesis and characterization of poly (acrylic acid)-graft-poly(vinylidene fluoride) copolymers and pH-sensitive membranes. Macromolecules 2002;35:673–9.

[38] S. Moharana, M.K. Mishra, B. Behera, R.N. Mahaling, A comparative study of dielectric properties of calcined and un-calcined BiFeO₃-poly (vinylidene fluoride) (PVDF) composite films, Int. J. Eng. Technol. Manage. Appl. Sci. 3(4), (2015), ISSN 2349–4476.

[39] A.K. Roy, A. Singh, K. Kumari, K. Prasad, A. Prasad, Electrical conduction in (Bi0.5Na0.5)0.94Ba0.06TiO3-PVDF 0–3 composites by impedance spectroscopy, IOSR J. Appl. Phys. (IOSR-JAP), e-ISSN: 2278–4861 3(5), (2013), 47–58.

[40] Luo H, Zhang D, Jiang C, Yuan X, Chen C, Zhou K. Improved dielectric properties and energy storage density of poly(vinylidene fluoride-co-hexa-fluoro-propylene) nanocomposite with hydantoin epoxy resin coated BaTiO. ACS Appl. Mater. Interfaces 2015;7:8061–9.

[41] Barber P, Balasubramanian S, Anguchamy Y, Gong S, Wibowo A, Gao H, Ploehn HJ, Loye H. Polymer composite and nanocomposite dielectric materials for pulse power energy storage. Materials 2009;2(1697–173):3. http://dx.doi.org/10.3390/ma2041697.

[42] Sharma M, Madras G, Bose. Phys. Chem. Chem. Phys. 2014;16:14792–9.

[43] Fan B-H, Zha J-W, Wang D-R, Zhao J, Dang Z-M. Experimental study and theoretical prediction of dielectric permittivity in BaTiO₃/polyimide nanocomposite films. Appl. Phys. Lett. 2012;100:092903.

[44] Mural PKS, Sharma M, Shukla A, Bhadra S, Padmanabhan B, Madras G, et al. Porous membranes designed from bi-phasic polymeric blends containing silver decorated reduced graphene oxide synthesized via a facile one-pot approach. RSC Adv. 2015;5(41):32441–51.

[45] Abdalla S. Electrical conduction through DNA molecule. Prog. Biophys. Mol. Biol. 2011;106(3):485–97.

[46] Abdalla S. Gaussian distribution of relaxation through human blood. Physica B 2011;406(3):584–7.

[47] Ying-Ju Yu, McGaughey Alan JH. Energy barriers for dipole moment flipping in PVDF-related ferroelectric polymers. J. Chem. Phys. 2016;144:014901. http://dx.doi.org/10.1063/1.4939152.

[48] J.L. Wang, X.J. Meng, J.H. Chu, Ferroelectric Materials-Synthesis and Characterization, book edited by Aime Pelaiz Barranco, ISBN 978-953-51-2147-3, Published: July 29, 2015 under CC BY 3.0 license.

[49] P. Debye, Ver. Deut. Phys. Gesell. 15, 777, 1913; reprinted 1954 in collected papers of Peter J.W. Debye Inter-science, New York.

[50] Ozkazanc E, Guney HY, Skay TO, Tarcan E. The effect of uniaxial orientation on the dielectric relaxation behavior of α-PVDF. J. Appl. Polym. Sci. 2008;109:3878–86.

[51] Sharma M, Madras G, Bose S. Process induced electroactive β-polymorph in PVDF: effect on dielectric and ferroelectric properties. Phys. Chem. Chem. Phys. 2014;16:14792–9.

[52] Bhingardive V, Sharma M, Suwas S, Madras G, Bose S. Polyvinylidene fluoride based lightweight and corrosion resistant electromagnetic shielding materials. RSC Adv. 2015;5(45):35909–16.

[53] B.J. Chu, X. Zhou, K.L. Ren, B. Neese, M.R. Lin, Q. Wang, Q.M. Zhang, A dielectric polymer with high electric energy density and fast discharge speed. Science 313 (2006), 334–336.

[54] Tomer V, Manias E, Randall CA. High field properties and energy storage in nano composite dielectrics of poly(vinylidene fluoride-hexafluoropropylene). J. Appl. Phys. 2011;110:044107.